Ionic Phases of Ammonia-Rich Hydrate at High Densities

Wan Xu,[1,2] Victor Naden Robinson,[3,4] Xiao Zhang,[1,2] Hui-Chao Zhang,[1,2] Mary-Ellen Donnelly,[5] Philip Dalladay-Simpson,[5] Andreas Hermann,[3] Xiao-Di Liu,[1] and Eugene Gregoryanz[1,3,5,*]

[1]*Key Laboratory of Materials Physics, Institute of Solid State Physics, HFIPS, Chinese Academy of Sciences, Hefei 230031, China*

[2]*University of Science and Technology of China, Hefei 230026, China*

[3]*Centre for Science at Extreme Conditions and School of Physics and Astronomy, University of Edinburgh, Edinburgh EH9 3FD, United Kingdom*

[4]*International Centre for Theoretical Physics, 34151 Trieste, Italy*

[5]*Center for High Pressure Science and Technology Advanced Research, Shanghai 201203, China*

(Received 29 June 2020; accepted 3 December 2020; published 6 January 2021)

Mixtures of ammonia and water are major components of the "hot ice" mantle regions of icy planets. The ammonia-rich ammonia hemihydrate (AHH) plays a pivotal role as it precipitates from water-rich mixtures under pressure. It has been predicted to form ionic high-pressure structures, with fully disintegrated water molecules. Utilizing Raman spectroscopy measurements up to 123 GPa and first-principles calculations, we report the spontaneous ionization of AHH under compression. Spectroscopic measurements reveal that molecular AHH begins to transform into an ionic state at 26 GPa and then above ~69 GPa transforms into the fully ionic $P\bar{3}m1$ phase, AHH-III, characterized as ammonium oxide $(NH_4^+)_2O^{2-}$.

DOI: 10.1103/PhysRevLett.126.015702

Ammonia and water have remarkable cosmic abundance and play prominent roles in constituting the interior structure of ice planets, e.g., Uranus and Neptune, and icy satellites such as *Titan* and *Triton* [1–3]. Their importance in planetary sciences led to considerable theoretical and experimental interest studying their properties at high densities [4–9]. The established experimental phase diagrams of pure ammonia and water are dominated by molecular phases, but if subjected to extreme conditions they adopt exotic ionic and superionic configurations [4–6,10–19]. The superionic states feature protons diffusing freely through the lattices formed by oxygen or nitrogen ions. The superionicity can be taken as thermally activated hydrogen mobility [12,19], while ammonia's self-ionization $2NH_3 \rightarrow (NH_4^+)(NH_2^-)$ can be seen as pressure activated hydrogen motion [13,14]. For the less exotic ice mixtures, the majority of previous work remains theoretical [11,20–25].

Ammonia and water are readily miscible and can form three stable stoichiometric compounds that exist in nature: ammonia dihydrate (ADH), ammonia monohydrate (AMH), and ammonia hemihydrate (AHH) with the ratios of ammonia to water 1:2, 1:1, and 2:1, respectively. Among these hydrates, the AHH mixture stands out: under specific pressure-temperature conditions, both AMH and ADH decompose into AHH and excess ice [26,27], as do other water-rich ammonia hydrates [28], while first-principles calculations find AHH to be the energetically most stable hydrate [24] at high pressures. This suggests an important role for AHH in any ammonia-water mixture under planetary conditions [23].

Upon compression at room temperature, x-ray diffraction (XRD) measurements found a transition from AHH-II to a body-centered cubic (bcc) phase at 19 GPa and another new structure at 25 GPa [29], albeit without a clear signature in Raman signals for the latter. Combined neutron and XRD experiments showed that deuterated AHH-II transforms into the bcc disordered molecular alloy (DMA) phase above 26 GPa and persists unchanged up to around 41 GPa [27], but also demonstrates significant kinetic effects via different sample preparation and compression routes.

First-principles calculations predicted that AHH will eventually transform from a hydrogen-bonded molecular solid into a fully ionic phase, ammonium oxide $(NH_4^+)_2O^{2-}$, above 65 GPa and to be stable in a sequence of ionic phases up to 500 GPa [23]. However, no further experimental studies have been reported, which leave the structures and properties of AHH at higher pressures unknown. In addition, spontaneous ionization of ADH [20] and AMH [11,21,22] were predicted theoretically, and a partial transformation of AMH into ammonium hydroxide $(NH_4^+)(OH^-)$ has been reported in a recent spectroscopy and diffraction study [30]. This stimulates our desire to explore the characteristics of AHH under compression and search for the ionic phases experimentally.

In this Letter, we report room temperature measurements of AHH up to 123 GPa by means of Raman spectroscopy and first-principles calculations. Above 26 GPa, spectroscopic measurements reveal AHH transforms to a partially ionized phase with ionic species characterized by the appearance of a high-energy vibrational peak assigned to

the N—H stretch of NH_4^+ in calculations [23]. Above 69 GPa, a phase transition to the predicted fully ionic AHH-III phase, with fully deprotonated waters, was observed. This phase remained stable to the highest pressure studied here. These intriguing ionic phases can exist over a considerably wide pressure region, and hence greatly extend the phase diagram of AHH. We also performed several XRD measurements to establish composition and aid structural confirmation (see the Supplemental Material [31] for details).

Figure 1 shows the evolution of the Raman spectra of the samples with pressure. At 300 K and below 4 GPa, in the liquid phase, three Raman-active vibrational peaks but no lattice modes are observed. At around 4 GPa, AHH solidifies to AHH-II, with the appearance of a series of low-frequency peaks, an O—H vibron at 3000 cm^{-1} and N—H vibron bands that occupy the range 3200–3420 cm^{-1}. Subsequently, at 29 GPa, a new peak appears at 3463 cm^{-1}, which hardens to 3624 cm^{-1} at 46 GPa. However, these peaks were eventually unable to be tracked as a broadband emerges around 3537 cm^{-1} at 69 GPa. The lattice modes exhibit a similar trend where only a broad weak band around 497 cm^{-1} can be observed. This is a suggestive feature of the DMA, as the variety of local environments lead to many different stretching frequencies

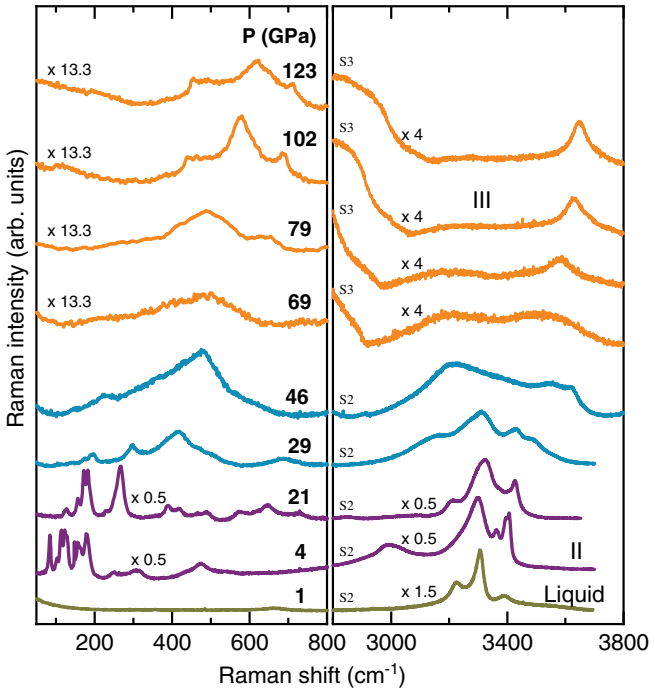

FIG. 1. Representative lattice modes and vibrational modes of Raman spectra for AHH at room temperature and different pressures. Different colors depict different phases. The shown spectra are from the different samples (S2 and S3). Additional details are provided in the Supplemental Material [31]. The scales for the intensity at low and high frequency are as indicated for each rescaled spectrum.

that form a band or continuous spectrum of vibrons, but below we make the case that a specific half-ionized AHH phase provides a good fit for these data. At 79 GPa, the spectra become more defined again and also simplify, as three lattice modes at 419, 507, and 656 cm^{-1} as well as two vibrational modes at 3196 and 3599 cm^{-1} and a shoulder at 3548 cm^{-1} can be distinguished. As the broad peak at 3196 cm^{-1} weakens, this mode reduces in intensity in calculations, while the peak at 3599 cm^{-1} sharpens and becomes more intense under compression. All peaks show a blueshift until our maximum investigated pressure, 123 GPa, where peaks at around 450, 620, 710, 3270, and 3650 cm^{-1} are identified.

In Fig. 2 we compare Raman peak positions with density-functional theory frequencies. After solidification, the vibron frequencies are in reasonable agreement with the calculations for AHH-II but are shifted by about 50 cm^{-1}, which could be attributed to anharmonic effects [49]. The O—H vibron mode at around 3000 cm^{-1} in AHH-II exhibits a strong softening under compression, a feature consistent with theoretical calculations that signals the weakening of the O—H covalent bond before the eventual ionization.

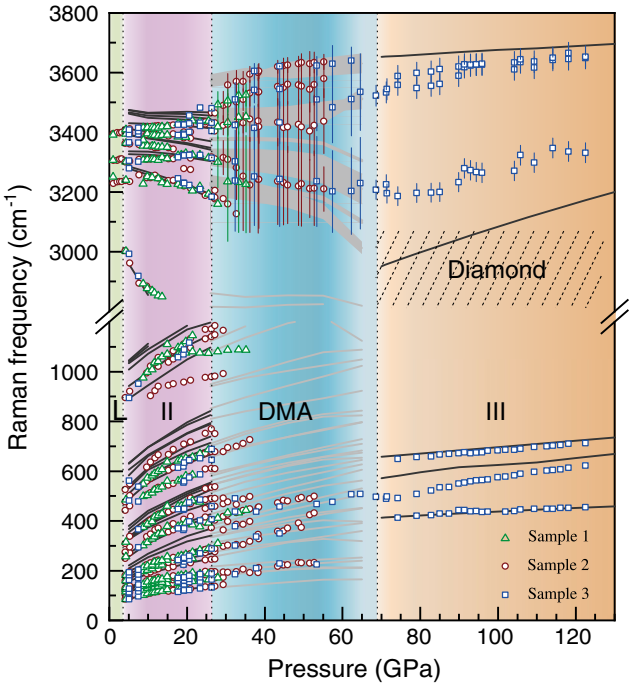

FIG. 2. Raman vibrational frequencies of AHH at room temperature from experimental results. Different colored symbols depict different runs (see legend). See Supplemental Material [31] for more sample details, including full width at half maximum as error bars for DMA high-frequency vibrons. Density-functional perturbation theory (DFPT) calculations are shown as black lines and gray regions as a function of pressure. Calculated frequencies for AHH-II* are shown in the DMA region with thickness related to the vibron intensity. The diagonal-dashed lines indicate the region where the sample signal may be covered by the Raman of second-order diamond.

Above 26 GPa the lattice modes change and the vibron region comes in two sections: the lower-frequency section with peaks at 3320 and 3200 cm^{-1} shows a redshift upon further compression, while the upper-frequency region remains constant or blueshifts under further compression. The former set of modes follow the general behavior of vibron frequencies in hydrogen-bonded solids softening under pressure [50]. Meanwhile, the latter set of vibron modes whose frequency increases rapidly to above 3600 cm^{-1} likely derives from the ionic N-H$\cdots$$NH_4^+$ hydrogen bonds, indicating the sample spontaneously starts to partially ionize in this pressure region. We find that these vibron spectra agree very well with calculations for the metastable and ordered quasi-bcc AHH-II* phase. By this we denote a partially ionic variant of AHH-II, where one proton in every water molecule has moved along a hydrogen bond, leading to an ordered 2/3 ionic (NH_4^+, OH^-) and 1/3 molecular (NH_3) structure with space group $P2_1/c$. The energy barriers for this proton transfer process are surprisingly small and vanish in calculations above 30 GPa (see Fig. 4 and Supplemental Material [31] for details). Note that a *second* proton transfer, from AHH-II* to a fully ionic ammonium oxide phase, also has an energy barrier that strongly decreases with pressure, eventually vanishes above around 60 GPa, and results in the AHH-III phase (see Fig. 4).

The observed lattice modes in the partially ionized pressure regime do not match as well with those of AHH-II* (see Fig. 2). Note that with increasing pressure AHH-II* must be metastable against the DMA phase, which has been established as the true thermodynamically stable phase in this region [27]. However, we find AHH-II* serves as a useful proxy for the simulated spectra of a quasi-bcc (DMA-like) and partially ionic phase, as it agrees particularly well in the vibron region. Measured DMA vibron peak positions in Fig. 2 are presented by the minimum number of peaks required to sufficiently fit the spectra. This pressure region can therefore be considered as partially ionized DMA, with possible coexistence of AHH-II*, where the characteristics of the DMA may drive the modes to gradually become indistinguishable and form a broadband. This explains why not all signals can be reproduced well by theoretical calculations.

Consistent with broadband formation, at 54 GPa we find that the higher-frequency vibron peaks merge into a single peak at 3482 cm^{-1}, while the peak at 3202 cm^{-1} remains roughly constant, and that the lattice modes merge into a single peak at 476 cm^{-1}. The merging of these peaks is consistent with a simplification of the structure.

At 69 GPa, the observed Raman frequencies qualitatively change again: two high-frequency modes as well as two new distinct lattice modes emerge and increase continuously with pressure, all of which closely resemble those of the predicted trigonal $P\bar{3}m1$ structure (see Fig. 2). This AHH-III phase, shown in Fig. 3, possesses the intriguing

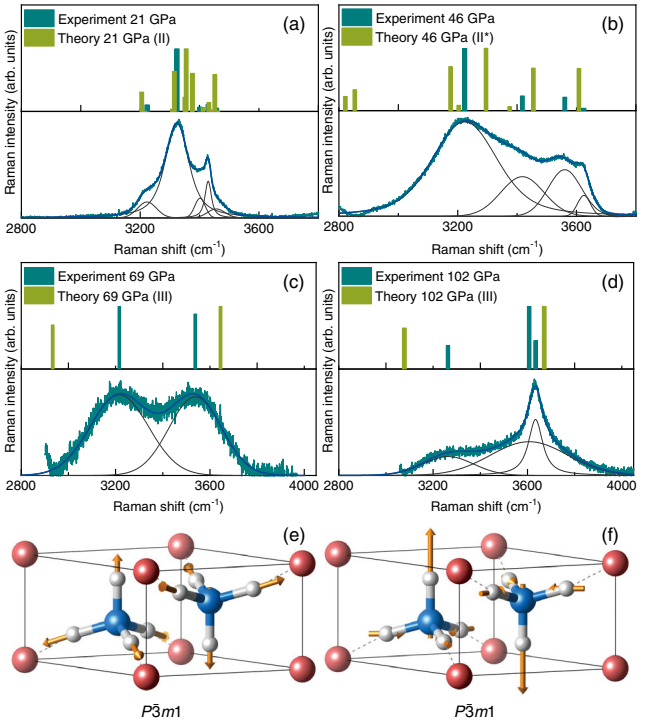

FIG. 3. (a)–(d) Raman spectra (lower) and renormalized fitted peak intensities compared with theoretical DFPT intensities (top), at four representative pressures. (e),(f) Crystal structure of AHH-$P\bar{3}m1$ at 100 GPa with Raman-active vibron displacement vectors for the (e) lower- and (f) higher-frequency N—H stretch modes. Red (blue, white) spheres denote O (N, H) atoms, respectively, and hydrogen bonds from NH_4^+ to O^{2-} are shown as dashed lines.

attribute of fully deprotonated water: all H_2O molecules have donated both protons to two NH_3 molecules, which results in a fully ionic ammonium oxide compound $(NH_4^+)_2O^{2-}$ [23]. It has two distinct Raman-active vibron modes (see Fig. 3 for the displacement patterns): a fully symmetric N—H stretch of the NH_4^+ units at lower frequency and an asymmetric N—H stretch at higher frequency. The calculated lower-frequency vibron is about 200 cm^{-1} below the observed 3200 cm^{-1} mode (and would not be visible in the spectra due to the signal of second-order diamond), but its pressure dependence (blueshift) agrees very well with the measured peak. Anharmonic effects can shift X-H vibrons by up to 200 cm^{-1} [49]. The higher-frequency vibron and all three lattice modes are in very good agreement with the data. A Rietveld refinement of the $P\bar{3}m1$ structure fits XRD data above 100 GPa (see Supplemental Material [31]).

Comparing experimental peak assignments, in particular, for broadband excitations, with harmonic frequencies can sometimes be misleading. In Fig. 3 we show Raman spectra and fitted peak positions and intensities vs calculated frequencies and intensities from DFPT-PBE in the vibron regions for the different phases (see the Supplemental

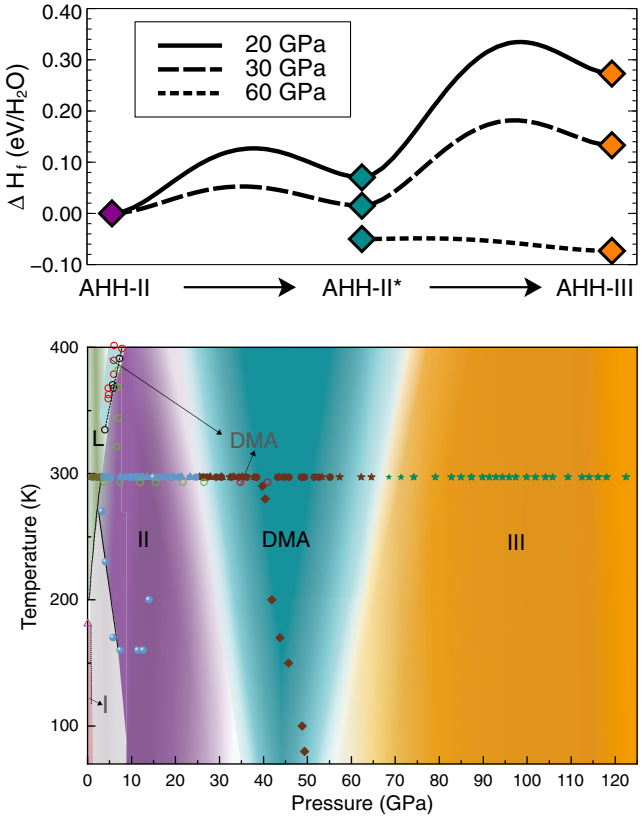

FIG. 4. Top: enthalpy change along a transition from AHH-II via AHH-II* to AHH-III, involving successive proton transfers from H_2O via OH^- to O^{2-}, at three different pressures. Bottom: the proposed phase diagram of AHH based upon this Letter and low-pressure data from Wilson *et al.* [27] (dashed lines below 10 GPa and unfilled circles, where red, green, black unfilled circles represent DMA, AHH-II, mixed phases, respectively). For our experimental data, different colors depict different phases, and different filled symbols represent different runs.

Material [31] for similar results from local density approximation calculations). The peak structure and relative intensities of AHH-II (21 GPa), AHH-II*/DMA proxy (46 GPa), and AHH-III (69 and 102 GPa) are all reproduced very well, giving further confidence to our assignments of these phases. The largest mismatch is the lower vibron peak in the AHH-III phase, which is underestimated by about 250 cm^{-1} at 69 GPa, compared to experiment; it is closer at higher pressure. Such disagreement could be due to anharmonic effects [49].

Combining previously reported data [27] with our experimental results, a phase diagram beyond megabar pressure for AHH is shown in Fig. 4. The top panel in Fig. 4 illustrates the energetics along one possible pathway to reach fully ionic high-pressure phases, via successive proton transfers along hydrogen bonds in AHH-II. At room temperature, AHH solidifies at around 4 GPa, forming AHH-II, followed by partially ionic DMA/AHH-II* above 26 GPa and finally the predicted fully ionic AHH-III above 69 GPa. Provisional phase boundaries are drawn to account for the fact that DMA is a configurationally disordered structure and so is likely favored at higher temperature over AHH-II and AHH-III. In previously reported studies, AHH-II transformed to the DMA phase under compression [27,29], which is consistent with our results. However, DMA did not form on all pressure-temperature pathways [27], suggesting kinetic barriers can retain AHH in metastable structures. AHH-II* shares the hydrogen bond topology and symmetry ($P2_1/c$ space group) with AHH-II; it has local distorted bcc features akin to DMA but is still ordered with far less variety of local environments. While it provides an intermediate metastable structure along a low-barrier transition pathway to the fully ionic $P\bar{3}m1$ phase (see Fig. 4), it also serves as a useful proxy for the spectroscopic properties of a partially ionic DMA-like phase. The partially and fully ionic phases exist over a comparatively wide pressure region and extend the AHH phase diagram considerably.

The present Letter highlights a fascinating mechanism of the self-ionization in AHH. Raman spectra up to 123 GPa reveal the molecular crystal spontaneously converting into an ionic state above 26 GPa as the measured Raman modes are in agreement with the presence of NH_4^+ species. A transition into the fully ionic $P\bar{3}m1$ phase was detected above 69 GPa, demonstrating for the first time that water molecules can completely disintegrate exclusively by applying pressure—unlike thermally activated decompositions in superionic phases of ice or ammonia, and also distinct from the atomic network phase of ice X.

Given the importance of the AHH composition amongst water-ammonia mixtures, exploring its exotic properties at extreme compression gives new important inputs for the interior modeling of icy planets.

This work was supported by National Natural Science Foundation of China (Grants No. 11874361, No. 51672279, No. 11774354, and No. 51727806), CAS Innovation Grant (No. CXJJ-19-B08), Science Challenge Project (Grant No. TZ2016001), and the CASHIPS Director's Fund (Grant No. YZJJ201705). Computational resources provided by the UK's National Supercomputer Service through the UK Car-Parrinello consortium (EP/P022561/1) and project ID d56 "Planetary Interiors" and by the UK Materials and Molecular Modelling Hub (EP/P020194) are gratefully acknowledged.

*e.gregoryanz@ed.ac.uk

[1] R. Helled, J. D. Anderson, M. Podolak, and G. Schubert, Astrophys. J. **726**, 15 (2011).
[2] G. Tobie, O. Grasset, J. I. Lunine, A. Mocquet, and C. Sotin, Icarus **175**, 496 (2005).
[3] A. Fortes, Icarus **146**, 444 (2000).

[4] M. Millot, S. Hamel, J. R. Rygg, P. M. Celliers, G. W. Collins, F. Coppari, D. E. Fratanduono, R. Jeanloz, D. Swift, and J. H. Eggert, Nat. Phys. **14**, 297 (2018).

[5] M. Millot, F. Coppari, J. R. Rygg, A. C. Barrios, S. Hamel, D. Swift, and J. H. Eggert, Nature (London) **569**, 251 (2019).

[6] C. Cavazzoni, G. Chiarotti, S. Scandolo, E. Tosatti, M. Bernasconi, and M. Parrinello, Science **283**, 44 (1999).

[7] R. Redmer, T. R. Mattsson, N. Nettelmann, and M. French, Icarus **211**, 798 (2011).

[8] L. Scheibe, N. Nettelmann, and R. Redmer, Astron. Astrophys. **632**, A70 (2019).

[9] L. Stixrude, S. Baroni, and F. Grasselli, arXiv:2004.01756.

[10] C. J. Pickard and R. Needs, Nat. Mater. **7**, 775 (2008).

[11] G. I. Griffiths, A. J. Misquitta, A. D. Fortes, C. J. Pickard, and R. J. Needs, J. Chem. Phys. **137**, 064506 (2012).

[12] S. Ninet, F. Datchi, and A. M. Saitta, Phys. Rev. Lett. **108**, 165702 (2012).

[13] S. Ninet, F. Datchi, P. Dumas, M. Mezouar, G. Garbarino, A. Mafety, C. J. Pickard, R. J. Needs, and A. M. Saitta, Phys. Rev. B **89**, 174103 (2014).

[14] T. Palasyuk, I. Troyan, M. Eremets, V. Drozd, S. Medvedev, P. Zaleski-Ejgierd, E. Magos-Palasyuk, H. Wang, S. A. Bonev, D. Dudenko *et al.*, Nat. Commun. **5**, 3460 (2014).

[15] Y. Wang, H. Liu, J. Lv, L. Zhu, H. Wang, and Y. Ma, Nat. Commun. **2**, 563 (2011).

[16] J.-F. Lin, E. Gregoryanz, V. V. Struzhkin, M. Somayazulu, H.-k. Mao, and R. J. Hemley, Geophys. Res. Lett. **32**, L11306 (2005).

[17] N. Goldman, L. E. Fried, I. Feng W. Kuo, and C. J. Mundy, Phys. Rev. Lett. **94**, 217801 (2005).

[18] J. Sun, B. K. Clark, S. Torquato, and R. Car, Nat. Commun. **6**, 8156 (2015).

[19] A. F. Goncharov, N. Goldman, L. E. Fried, J. C. Crowhurst, I. Feng W. Kuo, C. J. Mundy, and J. M. Zaug, Phys. Rev. Lett. **94**, 125508 (2005).

[20] X. Jiang, X. Wu, Z. Zheng, Y. Huang, and J. Zhao, Phys. Rev. B **95**, 144104 (2017).

[21] M. Bethkenhagen, D. Cebulla, R. Redmer, and S. Hamel, J. Phys. Chem. A **119**, 10582 (2015).

[22] A. D. Fortes, J. P. Brodholt, I. G. Wood, L. Vočadlo, and H. Jenkins, J. Chem. Phys. **115**, 7006 (2001).

[23] V. N. Robinson, Y. Wang, Y. Ma, and A. Hermann, Proc. Natl. Acad. Sci. U.S.A. **114**, 9003 (2017).

[24] V. Naden Robinson, M. Marqués, Y. Wang, Y. Ma, and A. Hermann, J. Chem. Phys. **149**, 234501 (2018).

[25] V. N. Robinson and A. Hermann, J. Phys. Condens. Matter **32**, 184004 (2020).

[26] C. Wilson, C. Bull, G. Stinton, and J. Loveday, J. Chem. Phys. **136**, 094506 (2012).

[27] C. Wilson, C. Bull, G. Stinton, D. Amos, M.-E. Donnelly, and J. Loveday, J. Chem. Phys. **142**, 094707 (2015).

[28] X. Li, W. Shi, X. Liu, and Z. Mao, Am. Mineral. **104**, 1307 (2019).

[29] C. Ma, F. Li, Q. Zhou, F. Huang, J. Wang, M. Zhang, Z. Wang, and Q. Cui, RSC Adv. **2**, 4920 (2012).

[30] C. Liu, A. Mafety, J. Queyroux, C. Wilson, H. Zhang, K. Beneut, G. Le Marchand, B. Baptiste, P. Dumas, G. Garbarino *et al.*, Nat. Commun. **8**, 1065 (2017).

[31] See Supplemental Material at http://link.aps.org/supplemental/10.1103/PhysRevLett.126.015702 for description of experimental and theoretical methods and analysis of samples and composition, which includes Refs. [32–48].

[32] D. D. Ragan, R. Gustavsen, and D. Schiferl, J. Appl. Phys. **72**, 5539 (1992).

[33] K. Syassen, High Press. Res. **28**, 75 (2008).

[34] G. Kresse and J. Furthmüller, Phys. Rev. B **54**, 11169 (1996).

[35] S. J. Clark, M. D. Segall, C. J. Pickard, P. J. Hasnip, M. I. J. Probert, K. Refson, and M. C. Payne, Z. Kristall. **220**, 567 (2005).

[36] P. Giannozzi, S. Baroni, N. Bonini, M. Calandra, R. Car, C. Cavazzoni, D. Ceresoli, G. L. Chiarotti, M. Cococcioni, I. Dabo *et al.*, J. Phys. Condens. Matter **21**, 395502 (2009).

[37] G. Kresse and D. Joubert, Phys. Rev. B **59**, 1758 (1999).

[38] D. R. Hamann, Phys. Rev. B **88**, 085117 (2013).

[39] M. J. van Setten, M. Giantomassi, E. Bousquet, M. J. Verstraete, D. R. Hamann, X. Gonze, and G. M. Rignanese, Comput. Phys. Commun. **226**, 39 (2018).

[40] J. P. Perdew, K. Burke, and M. Ernzerhof, Phys. Rev. Lett. **77**, 3865 (1996).

[41] J. P. Perdew and A. Zunger, Phys. Rev. B **23**, 5048 (1981).

[42] S. Baroni, S. De Gironcoli, A. Dal Corso, and P. Giannozzi, Rev. Mod. Phys. **73**, 515 (2001).

[43] K. Refson, P. R. Tulip, and S. J. Clark, Phys. Rev. B **73**, 155114 (2006).

[44] O. L. Anderson, D. G. Isaak, and S. Yamamoto, J. Appl. Phys. **65**, 1534 (1989).

[45] C. Prescher and V. B. Prakapenka, High Press. Res. **35**, 223 (2015).

[46] B. H. Toby and R. B. Von Dreele, J. Appl. Crystallogr. **46**, 544 (2013).

[47] Yuichi Akahama and Haruki Kawamura, J. Appl. Phys. **100**, 043516 (2006).

[48] C. Zha, W. Bassett, and S. Shim, Rev. Sci. Instrum. **75**, 2409 (2004).

[49] G. Gajewski, P. D. Mitev, and K. Hermansson, J. Chem. Phys. **129**, 064502 (2008).

[50] E. Libowitzky, in *Hydrogen Bond Research*, edited by P. Schuster and W. Mikenda (Springer, Vienna, 1999), pp. 103–115.